Proceedings of the CTD 2022
PROC-CTD2022-16
July 15, 2022

ATLAS Inner Detector alignment towards Run 3

Paolo Sabatini

On behalf of the ATLAS Collaboration,
Instituto de Fisica Corpuscular (IFIC)
Centro Mixto Universidad de Valencia - CSIC, Spain

ABSTRACT

The algorithm used in the alignment of the Inner Detector of the ATLAS experiment is based on the track-to-hit residual minimization in a sequence of hierarchical levels mimicking the detector assembly: from large mechanical structures to individual modules. It aims to describe the detector geometry and its changes in time as accurately as possible, such that the resolution is not degraded by an imperfect positioning of the signal hit in the track reconstruction. The ID alignment during Run 2 has proven to describe the detector geometry with a precision at the level of µm. Moreover, the hit-to-track residual minimization procedure is not sensitive to deformations of the detectors that affect the track parameters while leaving the residuals unchanged. Those geometry deformations are called weak modes. The minimization of the remaining track parameter biases and weak mode deformations has been the main target of the alignment campaign of the reprocessed Run 2 data. New analysis methods for the weak mode measurement have been therefore implemented, providing a robust geometry description, validated by a wide spectrum of quality-assessment techniques. These novelties are foreseen to be the new baseline methods for Run 3 data-taking, in which the higher luminosity would allow an almost real-time assessment of the alignment performance.

PRESENTED AT

Connecting the Dots Workshop (CTD 2022)
May 31 - June 2, 2022

1 Introduction

The enormous amount of data collected by the ATLAS experiment [1] at the LHC [2] in Run 2 (139 fb^{-1}) and expected for Run 3 (≈ 280 fb^{-1}) requires a precise reconstruction of the emerging products from Large Hadron Collider (LHC) collisions. The Inner Detector (ID) [3] tracking system must provide an accurate measurement of the positions of the charged particles as they cross its sensors to deliver a robust and precise reconstruction of the particle trajectory. A limited knowledge of the sensor position would turn into a degraded resolution of the position measurement or, in the worst case, a wrong reconstructed position. The precise determination of the ID geometry is therefore a crucial ingredient in all measurements using track information, from Standard Model processes to new physics searches.

In Run 2, the ID consisted of Pixel Detector [4], including the insertable B-Layer [5], a semiconductor tracker (SCT) [6] and a transition tracker (TRT), summing up to 750 000 degrees of freedom necessary to uniquely define its geometry down to single sensor position and orientation. The process of determining the ID geometry is called *alignment* [7]. The alignment procedure consists in the minimization of the track-hit residuals*. The procedure is organized in a sequence of hierarchical alignment levels addressing different structures of the detector from supporting structures to positions of the single sensor modules. The geometry of large structures is frequently measured as changing significantly within the LHC fill, while the module-level alignment is much more stable in time and requires less updates. This alignment procedure is however not sensitive to correlated distortions of the detector geometry (e.g. coherent rotation of the ID barrel layers). These distortions, called *weak-modes*, are of particular relevance as they may affect the track reconstruction.

During the LHC Long Shutdown 2, the ATLAS collaboration significantly improved the existing reconstruction algorithms to cope with the challenges of Run 3 data-taking [8]. One of the most prominent novelties was the replacement of the Neural Network used in Run 2 (Run 2 NN [9]) used in the estimation of the Pixel hit position and corresponding uncertainty. This was substituted by a *Mixture Density Network* (MDN) [10, 11]. The use of MDN removed a small bias in the reconstructed Pixel hits which translated in a change in the track-hit residuals. Consequently, a new alignment of the ID was necessary, as described in Section 2 [12]. Furthermore, a new technique was developed for the assessment of weak-modes affecting the reconstructed track momentum [12] and described in Section 3.

2 Inner Detector alignment campaign

The MDN algorithm was introduced in the Run 3 software suite for the track reconstruction as it outperforms the Run 2 NN in an environment with high hit occupancy, expected in Run 3 [10, 11]. Furthermore, it is not affected by a small bias in the position reconstruction as the Run 2 NN [12]. This bias on the reconstructed track position in local-y coordinate† in simulated events is shown in Figure 1a.

The NN position bias was absorbed by the alignment procedure through adjusting the detector geometry in Run 2. When these alignment constants are used in the track reconstruction with the new software suite exploiting the MDN algorithm, an opposite position bias appears in data events, as shown in Figure 1b. Therefore, a dedicated alignment was needed to remove the distortion introduced by the Run 2 NN bias.

Since the position bias had a strong dependence over the track position along the beam axis, a module-level alignment was required. Since the bias showed to be stable over time, see Figure 1b, only seven sets of constants were delivered to cover the whole Run 2 data-taking of pp collisions at $\sqrt{s} = 13$ TeV. Three sets

*A signal of a detector element generated by a crossing charged particle is called *hit*. The distance between the measured hit and the position in which the reconstructed track crosses the detector element is called *track-hit residual*.

†Local-y (local-x) coordinate is defined as the coordinate of the track or hit position on the sensor module in the direction of lower (higher) resolution. In this case, local-y (local-x) corresponds to the beam ($r\phi$) direction in the global coordinate system [7, 12].

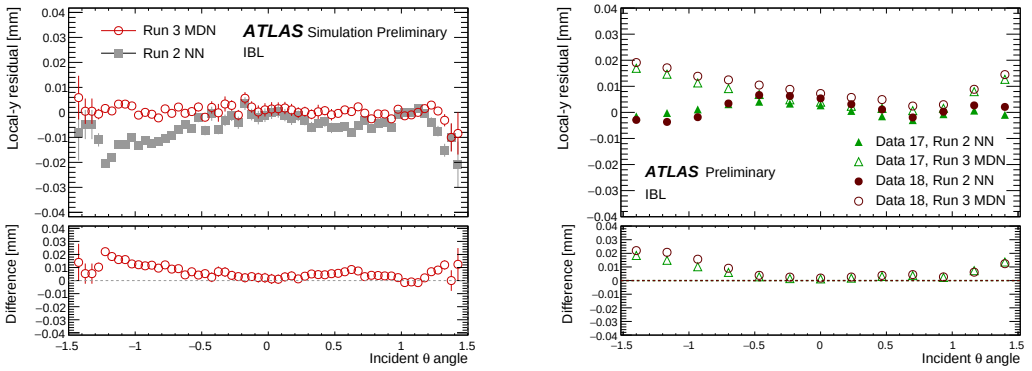

(a) (b)

Figure 1: Observed bias on the IBL track-hit residuals in the direction along the beam axis depending on the incident angle of the track into the Pixel mdoules. (a) The local-y residual in simulated events with the MDN algorithm (red) and Run 2 NN (gray). (b) The local-y residual in data events with the MDN algorithm (open markers) and Run2 NN (filled markers). Data events from 2107 data-taking are displayed in green, while data events from 2018 are displayed in purple. [12]

more were produced to cover special runs and heavy ion collision periods.

The alignment procedure consisted in two rounds. The first round aimed at the minimisation of the track-hit residual, that brought the mean of the residual distribution to be compatible with zero. The second round targeted the minimisation of the observed weak-modes, addressing a bias in the transverse impact parameter (d_0) and momentum. The bias in d_0 is assessed in data enriched of $Z \to \mu^+\mu^-$ events as a function of the (η, ϕ) coordinates of the muons. These values are used as constraints for the tracks used in the following iteration of the alignment procedure in order to adjust the detector geometry to minimize such bias. This procedure is repeated until convergence of the derived alignment constants is reached. The results of these two rounds in terms of track-hit residual minimization and d_0 bias removal are shown in Figure 2: despite the first round of alignment removed the bias in the local-y position, the second round was needed to remove the d_0 bias.

As mentioned above, the second round of alignment also aimed at the minimisation of a momentum bias, specifically in the measurement of sagitta. This bias was also quantified in $Z \to \mu^+\mu^-$ events, where the momenta of positive and negative muons are expected to be roughly the same. A sagitta bias δ_s alters the reconstructed momentum (p'_{T}) of a particle with respect to its original momentum (p_{T}) in a charge (q) dependent way according to:

$$p'_{\mathrm{T}} = p_{\mathrm{T}} \left(1 + q p_{\mathrm{T}} \delta_s\right)^{-1} \tag{1}$$

The presence of δ_s introduces a bias in the p_{T} distributions of positive and negative in opposite directions, as shown in Figure 3a. The discrepancy of the mean values of the positive (p^+_{T}) and negative (p^-_{T}) momentum distributions is used to estimate δ_s with:

$$\delta_s = -\frac{1}{\langle p_{\mathrm{T}} \rangle} \frac{\langle p^+_{\mathrm{T}} \rangle - \langle p^-_{\mathrm{T}} \rangle}{\langle p^+_{\mathrm{T}} \rangle + \langle p^-_{\mathrm{T}} \rangle} \tag{2}$$

The extracted value of the measured sagitta bias is used as constrain of the tracks in the alignment iterations described above. The reduction of the sagitta bias is evident in Figure 3b. This procedure has shown not to cancel any physics-motivated momentum asymmetry in data events, as shown in Figure 3c. The forward-backward asymmetry (A_{FB}) [13] in $Z \to \mu^+\mu^-$ events is observed also in data after the alignment procedure as in simulated events, while the "wiggle" due to the presence of a sagitta bias is reduced.

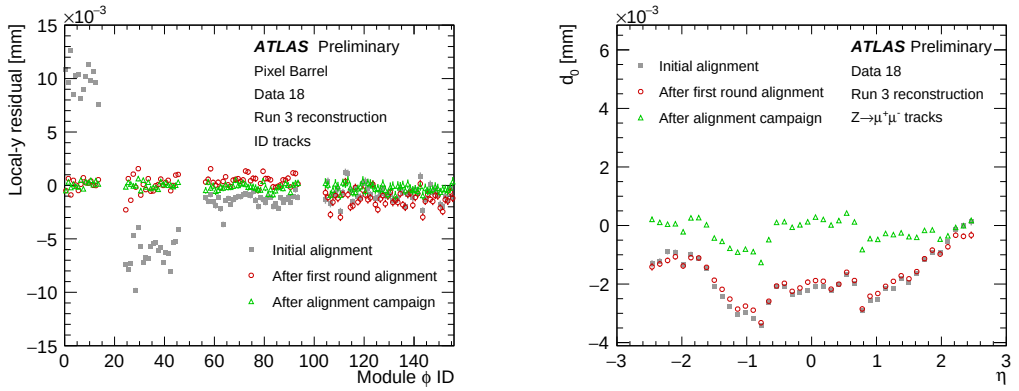

(a) (b)

Figure 2: Observed biases in the alignment procedure. Grey points indicate the initial conditions, the red points stand for the results of the first alignment round using only track-hit residual minimization, and the green points show the results of the alignment that uses constrains on the track parameters. (a) Track-hit residuals in the IBL and Pixel detectors. There are 4 group of points that correspond to the IBL, and then the 3 layers of the Pixel system. The points in each group correspond to the different ladders of modules segmented in ϕ. (b) Profile of the transverse impact parameter (d_0) versus the track . [12]

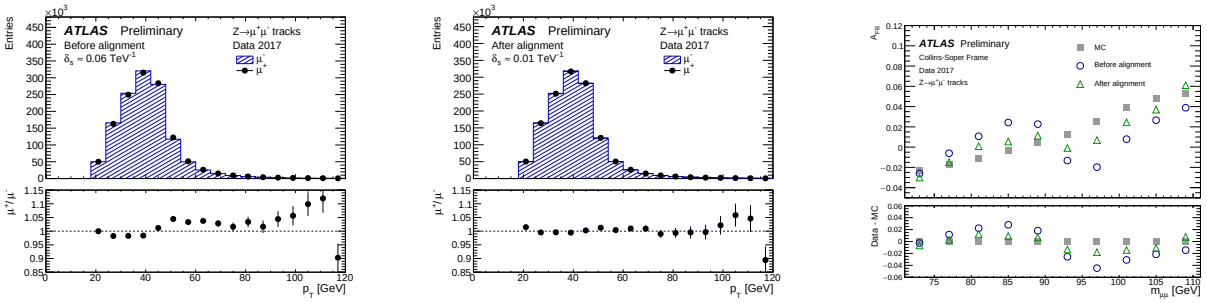

(a) (b) (c)

Figure 3: Comparison of the p_{T} spectrum of the positive and negative muons in $Z \to \mu^+\mu^-$ events (a) before using track parameter constraints in the alignment and (b) after the alignment round with track parameter constraints. (c) Reconstructed forward-backward asymmetry(A_{FB}) using the Collins-Soper frame [13] in $Z \to \mu^+\mu^-$ events in MC and data events from 2017. The plot shows the values for the asymmetry before (blue) using track parameter constraints in the alignment and after (green) the alignment round with track parameter constraints. [12]

The performance of the alignment constants are quantified in terms of remaining biases in the track parameters using a sample of $Z \to \mu^+\mu^-$ in data. The difference in the transverse (longitudinal) impact parameter between the positive and negative muon δd_0 (δz_0) are shown in Figure 4a (Figure 4b) to be well below 1 μm (5 μm). Robust physics performances is observed during Run 2, as shown from the stable value of the di-muon reconstructed mass over time in Figure 4c.

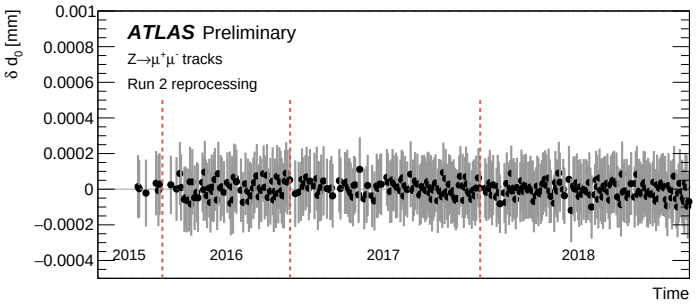

(a)

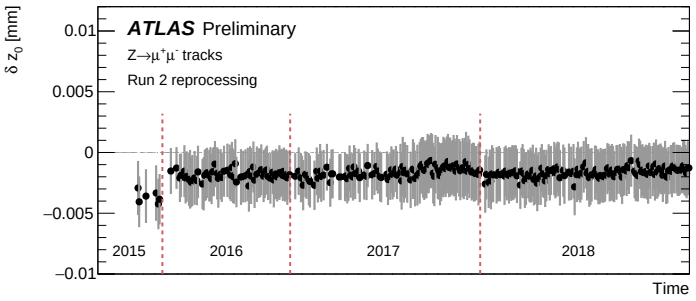

(b)

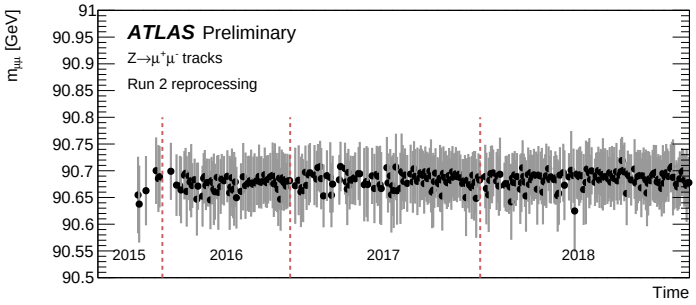

(c)

Figure 4: Remaining biases in the (a) transverse and (b) longitudinal impact parameter after the alignment campaign versus the time during Run 2. (c) Reconstructed mass of the di-muon system versus the time during Run 2. [12]

3 New method for sagitta bias measurement

The value of the extracted sagitta bias measured with Equation 2 is intended as *global bias*, as it affects the mean of the distribution. Local gradients of the bias over the detector are instead indicated as *relative bias*. In the past, the alignment procedure used two methods to assess them separately. The ratio of the measurements of energy in the calorimeter and momentum in the ID of electrons from Z boson decay was used to measure the global sagitta bias (E/p method) [7]. A *Mass* method [7] was instead implemented to measure the relative bias. Equation 2 provided an estimation of the global sagitta bias without the use of a

completely different sample of events and therefore preferred over the E/p method.

Since this procedure was not optimal, a new method has been developed to measure both global and relative bias simultaneously. The method is based on $Z \to \mu^+\mu^-$ events and differs from the existing *Mass* method on the choice of the figure of merit to be minimised to measure the bias. The *Mass* method is based on the minimisation of the difference between the reconstructed di-muon mass $m_{\mu\mu}$ and a reference mass ($m_{\mu\mu,0}$). From Equation 1, this difference can be written as:

$$\frac{m^2_{\mu\mu} - m^2_{\mu\mu,0}}{m^2_{\mu\mu}} = (p^-_{\mathrm{T}}\delta^- - p^+_{\mathrm{T}}\delta^+) \tag{3}$$

where $\delta^{+/-}$ stands for the bias affecting the reconstruction of the positive and negative muon momenta ($p^{+/-}_{\mathrm{T}}$). In case of a global bias ($\delta^+ \approx \delta^-$) in $Z \to \mu^+\mu^-$ events (in which $\langle p^+_{\mathrm{T}}\rangle \approx \langle p^-_{\mathrm{T}}\rangle$), the difference $m^2_{\mu\mu} - m^2_{\mu\mu,0} \approx 0$. Therefore, the *Mass* method can not be sensitive to a global sagitta bias. Conversely, the width of the reconstructed di-muon mass distribution would increase in presence of a global (and/or relative) sagitta bias. The new *VarMin* method [12] exploits this behaviour and measures the sagitta bias by minimising the width of the reconstructed di-muon mass. The mathematical derivation, documented in Ref. [12] resolves in the solution of a N-dimensional system of linear equation, where N stands for the number of sections in which the detector is segmented in the (η, ϕ) coordinates. The unknown $\vec{\delta}$ consists in the values of the sagitta bias in each section of the detector that minimise the overall width of the di-muon mass distribution.

The measured sagitta values on the same set of data events using the *VarMin* and *Mass* methods are shown in Figure 5a and 5b, respectively. The results are almost identical as indicated by the high correlation factor shown in Figure 5c. This result also indicates that the level of the global sagitta bias is almost negligible after the alignment campaign as *VarMin* method is expected to be sensitive to it, while the *Mass* method is not. The value of the sagitta bias during Run 2 data-taking is shown in Figure 6, showing to be below 0.1 TeV^{-1} over the detector for the whole Run 2 with a mean value (i.e. global bias) around 0.02 TeV^{-1}.

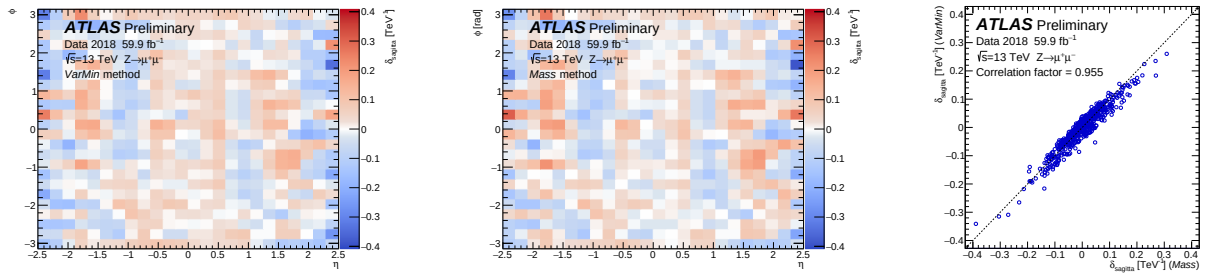

(a) (b) (c)

Figure 5: Measured sagitta bias (η, ϕ) maps from $Z \to \mu^+\mu^-$ data events from 2018 data-taking as obtained with the *Mass* (a) and *VarMin* (b) methods. The detector is split in 24×24 uniformly spaced (η, ϕ) sectors. (c) Comparison of the sagitta bias as computed with the *Mass* and *VarMin* methods. Each point has as coordinates the computed sagitta bias with each method for the same (η, ϕ) sector. [12]

Eventually, the *VarMin* method outperforms the *Mass* method in terms of execution time. Both methods use iterations over the set of events in order to converge to the final measured value of sagitta bias. As shown in Figure 7, while the *Mass* method needs almost six iterations to obtain negligible corrections, the *VarMin* method converges in three iterations, drastically reducing the execution time.

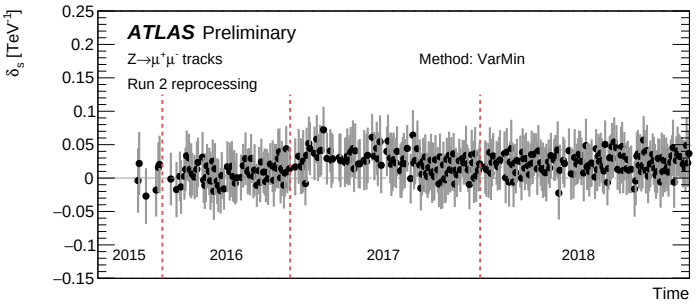

Figure 6: The sagitta bias on tracks, measured in $Z \to \mu^+\mu^-$ events following the VarMin method and for the data from the Run 2. [12]

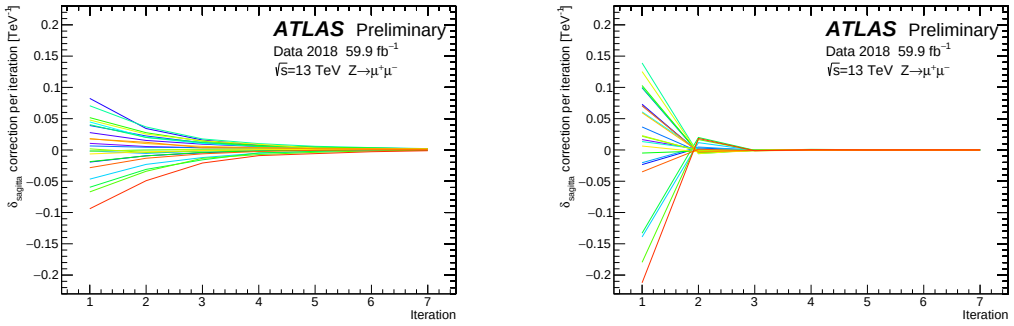

(a) (b)

Figure 7: Corrections of the sagitta bias per iteration using (a) *Mass* and (b) *VarMin* methods. Each line shows the sagitta bias computed for a given (η, ϕ) cell. For the sake of clarity, only a fraction of the total number of cells are drawn: just the 24 cells of the 12th row ($\phi \approx 0$) in Figure. 5. The line colors are used to distinguish each cell. [12]

4 Conclusions

The accurate determination of the geometry of the ATLAS tracking system plays an important role both in high-precision measurements of the Standard Model as well as in searches of new physics. A poor knowledge of the position and orientation of the detector elements affects the track reconstruction and ultimately physics measurement. The ATLAS alignment procedure of the Inner Detector has proven to deliver a robust description of the detector geometry and minimise the bias on the track parameters during Run 2.

The ATLAS reconstruction software suite has been renewed during the Long Shutdown 2 in order to improve the performances of the implemented algorithm in preparation of Run 3. The inclusion of a new algorithm (MDN) for the hit position estimation induced a movement of the track-hit residuals, calling for a new alignment campaign. New alignment constants covering the whole Run 2 data-taking have been delivered to be used within the new reconstruction software suite for improved analysis of Run 2 dataset and future combination with Run 3 data. The delivered description of the geometry has proven to minimise the biases on the track parameters down to a negligible level.

Weak-modes are coherent deformation of the detector geometry that are not caught by the alignment

procedure. Methods based on resonance decays are used to estimate them and used as input for the alignment algorithm to adjust the geometry to minimise them. A new method for the measurement of charge-dependent momentum biases (sagitta biases) is implemented, the *VarMin* method. This method outperforms the existing *Mass* method as it is sensitive to global biases and requires almost half the execution time to provide consistent results. This improvement is expected to be of a great importance in Run 3 of the LHC as it is planned to be used in the alignment iterations, so that a quick, automatic and accurate minimization of the sagitta bias during the alignment iterations will be possible.

References

[1] ATLAS Collaboration, *The ATLAS Experiment at the CERN Large Hadron Collider*, 2008 JINST **3** S08003, url: https://link.springer.com/article/10.1140/epjc/s10052-020-08700-6.

[2] L. Evans and P. Bryant, *LHC Machine*. 2008 JINST **3** S08001, url: https://iopscience.iop.org/article/10.1088/1748-0221/3/08/S08001.

[3] ATLAS Collaboration, *ATLAS Inner Detector: Technical Design Report*, Volume 1, ATLAS-TDR-4; CERN-LHCC-97-016, 1997, url: https://cds.cern.ch/record/331063.

[4] ATLAS Collaboration, *ATLAS Pixel Detector: Technical Design Report*, ATLAS-TDR-11; CERN-LHCC-98-013, 1998, url: https://cds.cern.ch/record/381263.

[5] B. Abbott et al., *Production and integration of the ATLAS Insertable B-Layer*, JINST **13** (2018) T05008, arXiv: 1803.00844 [physics.ins-det].

[6] ATLAS Collaboration, *ATLAS Inner Tracker Strip Detector: Technical Design Report*, ATLAS-TDR-025; CERN-LHCC-2017-005, 2017, url: https://cds.cern.ch/record/2257755.

[7] ATLAS Collaboration, *Alignment of the ATLAS Inner Detector in Run-2*, Eur. Phys. J. C **80** (2020) 1194, arXiv: 2007.07624 [hep-ex].

[8] ATLAS Collaboration, *Software Performance of the ATLAS Track Reconstruction for LHC Run 3*, ATL-PHYS-PUB-2021-012, 2021, url: https://cds.cern.ch/record/2766886.

[9] ATLAS Collaboration, *A neural network clustering algorithm for the ATLAS silicon pixel detector*, JINST **9** (2014) P09009, arXiv: 1406.7690 [hep-ex].

[10] ATLAS Collabroration, *ATLAS pixel cluster splitting using Mixture Density Networks*, ATL-PHYS-PROC-2019-082, CERN, 2019, url: https://cds.cern.ch/record/2687968..

[11] ATLAS Collaboration, *ATLAS pixel cluster splitting using Mixture Density Networks*, IDTR-2019-006, url: https://atlas.web.cern.ch/Atlas/GROUPS/PHYSICS/PLOTS/IDTR-2019-006/

[12] ATLAS Collaboration, *Inner Detector alignment development and performance in preparation for Run 3*, ATL-PHYS-PUB-2022-028, url: https://cds.cern.ch/record/2811212.

[13] J. C. Collins and D. E. Soper, *Angular distribution of dileptons in high-energy hadron collisions*, Phys. Rev. D **16** (7 1977) 2219, url: https://link.aps.org/doi/10.1103/PhysRevD.16.2219.